ResearchGate

See discussions, stats, and author profiles for this publication at: https://www.researchgate.net/publication/261949280

Decalin Loop in an Optimized Thermally Coupled Dual Methanol Reactor Using Differential Evolution (DE) Strategy

ARTICLE *in* ENERGY & FUELS · SEPTEMBER 2012

Impact Factor: 2.79 · DOI: 10.1021/ef300577m

CITATIONS
2

READS
24

5 AUTHORS, INCLUDING:

Salman Amiri
Allameh Tabatabai University
12 PUBLICATIONS **22** CITATIONS
SEE PROFILE

Azadeh Mirvakili
Shiraz University
20 PUBLICATIONS **122** CITATIONS
SEE PROFILE

Davood Iranshahi
Amirkabir University of Technology
50 PUBLICATIONS **391** CITATIONS
SEE PROFILE

M. R. Rahimpour
Shiraz University
331 PUBLICATIONS **3,022** CITATIONS
SEE PROFILE

Available from: M. R. Rahimpour
Retrieved on: 04 February 2016

energy&fuels

Article

pubs.acs.org/EF

Decalin Loop in an Optimized Thermally Coupled Dual Methanol Reactor Using Differential Evolution (DE) Strategy

Razieh Rafiei, Shahram Amiri, Azadeh Mirvakili, Davood Iranshahi, and Mohammad Reza Rahimpour*

School of Chemical and Petroleum Engineering, Department of Chemical Engineering, Shiraz University, Shiraz 71345, Iran

ABSTRACT: Decalin can be used as an energy carrier and hydrogen storage. This paper conducts an analysis of the decalin looping approach in optimized thermally coupled dual methanol reactor (OTCDMR) for simultaneous hydrogen production and consumption. This configuration takes the advantages of couple technique and membrane technology simultaneously. In the first reactor, methanol synthesis and decalin dehydrogenation take place in the tube and the shell sides, respectively. In the second one, naphthalene hydrogenation occurs in the tube side to produce decalin. In this configuration, the hydrogen obtained from the other sources such as a natural-gas steam reforming unit is entered to the second reactor for hydrogenation of naphthalene. Therefore, hydrogen can be stored in the storage tank by being converted into decalin as a liquid material with a high storage capability. The performance of OTCDMR is compared with the thermally coupled reactor (TCR) and the conventional reactor (CR). Results show that the methanol yield can increase about 5.8% and 9.5% in OTCDMR as compared with TCR and CR, respectively. The differential evolution (DE) strategy is used to optimize the configuration operating conditions by considering four decision variables.

1. INTRODUCTION

Today, fossil energy carriers are regarded as the main energy sources. Undoubtedly, due to the globally increasing use of energy, fossil fuels cannot persist for a long time. Considering this issue, the efficiency of energy utilization and resources should be improved.[1] In this work, we take the advantages of hydrogen carrier characteristics, coupling technique, membrane technology, and differential evolution strategy (one of the optimization methods). Therefore, the introduction section is divided into some orderly subsections, each of which clarifies one specific aspect of this contribution. An explanation of methanol synthesis as the major production is also presented.

1.1. Coupling Technique. The coupling of the endothermic and exothermic reactions can save energy, decrease reactor investments, increase thermal efficiency, and enhance the equilibrium conversion and reaction rate for reversible reactions. By utilizing the coupling of exothermic and endothermic reactions, the plant complexity will increase. Moreover, a number of separation units and recycles are required. However, energy saving and reduced reactor investments are more important than the cost of the additional units.[2] The coupling technique can be done in the three reactor configurations: recuperative coupling, direct coupling, and regenerative coupling. Ramaswamy et al. compared the performance of counter-current and cocurrent heat exchanger reactors by the one-dimensional pseudo-homogeneous plug flow model.[3] Ramaswamy et al. also used one-dimensional pseudo-homogeneous plug flow model to assess the performance of coupling exothermic and endothermic reactions in the directly coupled adiabatic packed bed reactor.[4] A reverse flow reactor, coupling endothermic and exothermic reactions, was investigated by Sint Annaland et al.[5]

1.2. Methanol Synthesis. Methanol is one of the major chemical products that is known as a clean-energy resource and a chemical feed stock.[6] The first methanol commercial implementation was in 1923, although its production technology has been improved greatly, methanol is still predominantly produced from synthesis gas. Synthesis gas is a mixture of H_2, CO, CO_2, and some inert gases such as nitrogen and methane.[7,8] A vertical shell and tube heat exchanger is basically used as a conventional methanol reactor.[9] A number of investigations have been carried out to improve the methanol reactor and increase its production. Maneti et al. conducted a study proposing and comparing different steady-state models for the methanol synthesis fixed bed reactor.[7] A new technology for methanol synthesis is presented by Rahimpour et al. This technology uses a dual-type reactor system rather than a single-type reactor.[10]

1.3. Hydrogen Carrier (Decalin). A number of factors, including the climate change, local air pollution, need to decrease green house emissions, and shortage of fossil fuels have caused scientists to search an alternative clean energy source.[1] Hydrogen has received special attention as an ideal energy carrier because of its fascinating properties, such as being highly efficient and free from pollution.[11] The reversible dehydrogenation−hydrogenation of the so-called liquid "organic hydrides" is one of the potential systems to store and transport hydrogen in a nongaseous infrastructure manner.[12] Substances that possess these sorts of characteristics are called hydrogen carriers. The combination of cycloalkane/cycloalkene systems such as the decalin/naphthalene and cyclohexane/benzene systems has been proposed as an effectual carrier of hydrogen. Cooper et al.[13] investigated the probability of using the liquid phase cycloalkane hydrogen carriers (cyclohexane, methylcyclohexane, decalin, tetralin, etc.) to store and supply hydrogen. Hodoshima et al.[14] investigated dehydrogenation of decalin at 210 °C with carbon supported Pt catalysts in a batch

Received: April 5, 2012
Revised: July 28, 2012
Published: July 30, 2012

ACS Publications © 2012 American Chemical Society

dx.doi.org/10.1021/ef300577m | Energy Fuels 2012, 26, 5858−5871

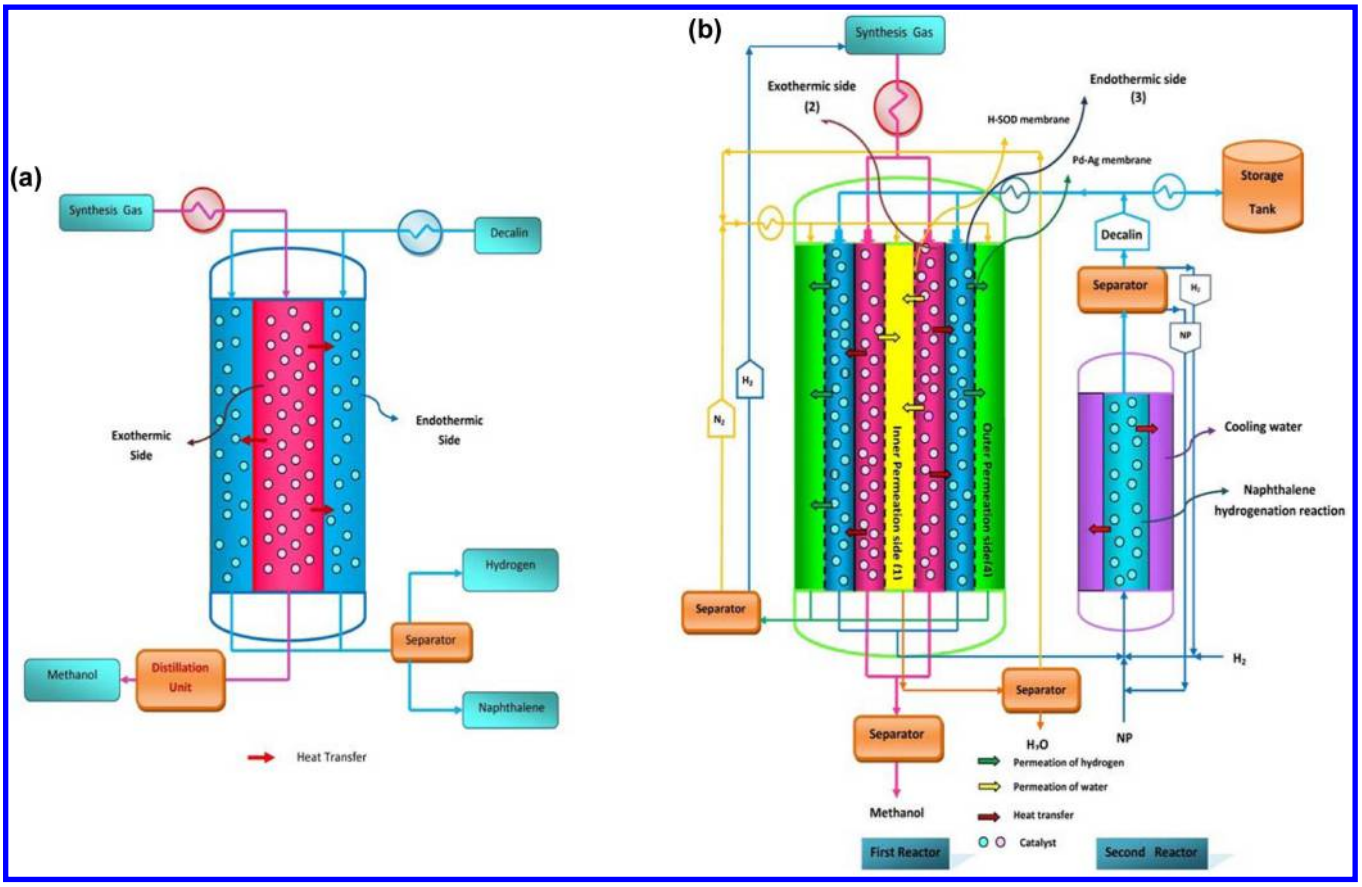

Figure 1. Schematic diagram of (a) thermally coupled reactor (TCR) and (b) optimized thermally coupled dual methanol reactor (OTCDMR).

reactor. Hydrogen was evolved from decalin much more efficiently than the suspended states due to the superheated states of the dehydrogenation catalyst. Froment et al.[15] investigated the dehydrogenation of decalin for the production of pure hydrogen for fuel cell applications. It is attainable to have about 98% conversion with more than 99.9% selectivity for the dehydrogenation reaction by using supported Pt catalysts. Naphthalene and hydrogen are produced from dehydrogenation of decalin.

1.4. Pd−Ag and H-SOD Membranes. The membrane concept is a well-known technology for separation. Separation by membrane is less energy intensive and requires no phase change in the process.[16] By removing reactants from product gases, the equilibrium compositions shift toward the product;[17] therefore, membranes can be used to increase the reactions yield. Recently, the reaction systems that contain hydrogen and oxygen and that are based upon inorganic membranes have received special attention to use the membrane technology.[18] The Pd−Ag membrane layer with silver content of 23−25% is widely utilized for hydrogen purification.[19,20] Iranshahi et al. used a Pd−Ag membrane reactor for several investigations to extract hydrogen from the reaction region.[21,22] H-SOD (hydroxy sodalite) membrane is a zeolite-like material that consists of sodalite cages and is used for the water permeation.[23,24]The mechanical stability and thermal of H-SOD membrane are acceptable and the selectivity of water to hydrogen is excellent by using H-SOD.[25]

1.5. Optimization. One of the main difficulties associated with using traditional optimization techniques, which are based on gradient methods, is the probability of getting trapped at local optimums because of their sensitivity to initial guess. Therefore, finding a global optimum is not ensured by utilizing these methods. In the recent past, some advanced systems based on natural phenomena (evolutionary computation) such as simulated annealing (SA),[26] evolution strategies (ESs),[27] genetic algorithms (GAs),[28] and differential evolution (DE)[29] have been developed. One of the merits of utilizing the aforementioned methods, unlike traditional optimization techniques, is that they do not rely on a wide problem formulation to solve optimization problems. Among these methods, DE is used in various fields due to its simplicity, easiness of use, effectiveness as an evolution method, its reliance on few control variables, and finally its higher chance to find true global optimum for objective function.[29] In several studies, the DE method has been successfully used as the optimization technique, such as optimization of an alkylation reaction,[30] optimization of nonlinear chemical process,[31] optimal design of shell and tube heat exchanger,[32] and estimation of heat transfer parameters in trickle bed reactor.[33]

1.6. Objectives. The main goals of this work are to produce a higher amount of methanol and to investigate the possibility of using decalin as an energy carrier and hydrogen storage. In this work, a configuration consisting of two reactors for simultaneous decalin and hydrogen production and consumption is proposed. Methanol synthesis and decalin dehydrogenation take place in the first reactor and naphthalene hydrogenation occurs in the second reactor. In this configuration, the hydrogen storage problem can be solved because the hydrogen could be converted into decalin, as a material which is capable of being stored. The operating conditions are optimized by the DE method to maximize the methanol and hydrogen yield in the first reactor and decalin

dx.doi.org/10.1021/ef300577m | Energy Fuels 2012, 26, 5858−5871

yield in the second reactor. In addition, a comparison between optimized thermally coupled dual methanol reactor (OTCDMR), thermally coupled reactor (TCR), and the conventional methanol reactor is made to show the OTCDMR advantages such as achieving a higher amount of hydrogen, naphthalene, and methanol.

2. PROCESS DESCRIPTION

In the previous research work,[34] the CR configuration characteristics were widely elaborated. The schematic diagrams of TCR and OTCDMR are presented in Figure 1. TCR is a thermally coupled reactor that consists of a tube section surrounded by a shell section. In this reactor, it is assumed that the decalin dehydrogenation takes place in the shell side rather than cooling water. Heat is transferred from the methanol synthesis to decalin dehydrogenation, and several products (methanol, naphthalene and hydrogen) are obtained. The OTCDMR is an optimized thermally coupled dual methanol reactor. It consists of a thermally coupled membrane reactor followed by a vertical shell and tube heat exchanger. The reactions in the first reactor of this configuration are the same as those in TCR. Unlike the TCR, which cannot make use of decalin as an energy carrier and hydrogen storage, OTCDMR can use these decalin properties to solve hydrogen storage problem because of utilizing the second reactor, in which decalin is proposed as a hydrogen carrier. The cooling water is used in the second reactor to remove the heat, which is generated by decalin producing process. Moreover, by assisting H-SOD and Pd−Ag membrane layers in the methanol and naphthalene production regions, respectively, their production rates increase in OTCDMR. The H-SOD membrane shifts the equilibrium compositions toward the products in the methanol reaction by removing water. The Pd−Ag membrane layer performs this process in the naphthalene production region via extracting H_2; therefore, the methanol and naphthalene production quantities are in their highest values in OTCDMR. The hydrogen extracted via membrane leaves the first reactor, and after separating from N_2, it is used as some part of the hydrogen that is needed for the methanol synthesis (extracted H_2 is about 35% of the required hydrogen for methanol synthesis). Also, similar to the extracted hydrogen, the separated N_2 after separation can be used in this system. It is used as the sweeping gas in the membrane sections. The naphthalene and hydrogen that are produced in the first reactor via the endothermic reaction leave the reactor and are mixed with hydrogen (0.219 mol/s) and naphthalene (0.071 mol/s) streams coming from other sources and then enter the tube side of the second reactor. In the second reactor, hydrogen and naphthalene are converted into decalin (a liquid material with a high storage capability). As the naphthalene hydrogenation is exothermic, the generated heat is removed by cooling water. An amount of second-reactor exit decalin is used as an inlet feed of the first-reactor endothermic side, and the remaining part after the phase change can be stored in the storage tank to be used in the other petrochemical units as a hydrogen source. A separator is situated at the outlet of the second reactor to purify decalin, because the naphthalene hydrogenation does not take place completely. The separator separates hydrogen, decalin, and naphthalene, and then, the separated hydrogen and naphthalene are added to the feed of the second reactor. The

Table 1. Operating Conditions for Methanol Synthesis Process in TCR and OTCDMR First-Reactor

param.	value
feed comp. (mole fraction)	
CH_3OH	0.0050
CO_2	0.0940
CO	0.0460
H_2O	0.0004
H_2	0.6590
N_2	0.0930
CH_4	0.1026
total molar flow rate (mol s^{-1})	0.64
inlet pressure (bar)	76.98
inlet temp. of TCR (K)	503
inlet temp. of OTCDMR (K)	505.1
particle diam. (m)	5.47×10^{-3}
specific surface area (m^2 m^{-3})	626.98
bed void fraction	0.39
density of catalyst bed (kg m^{-3})	1140

Table 2. Operating Conditions for Dehydrogenation of Decalin to Naphthalene Process in TCR and OTCDMR and the Permeation Sides in OTCDMR

param.	value
feed comp. (mole fraction)	
trans-decalin (TDC)	0.764
cis-decalin (CDC)	0.236
total molar flow rate (mol s^{-1})	0.1
inlet pressure (bar)	1
inlet temp. of TCR (K)	503
inlet temp. of OTCDMR (K)	502
bed void fraction	0.39
Water Permeation Side	
feed comp. (mole fraction)	
N_2 (sweep gas)	1.0
H_2O	0.0
total molar flow rate (mol s^{-1})	1.0
inlet temp. (K)	503
inlet pressure (bar)	0.1
Hydrogen Permeation side	
feed comp. (mole fraction)	
N_2 (sweep gas)	1.0
H_2	0.0
total molar flow rate (mol s^{-1})	1.0
inlet temp. (K)	503
inlet pressure (bar)	0.1

Table 3. Characteristics of OTCDMR Reactor

param.	value
inner tube or permeation side diam. (m)	0.038
second tube or exothermic side diam. (m)	0.053
third tube or endothermic side diam. (m)	0.067
outer tube or permeation side diam. (m)	0.076
length of reactor (m)	7.022
inner membrane thickness (m)	6×10^{-6}
outer membrane thickness (m)	6×10^{-6}
Fixed-Bed Reactor (The Second Reactor)	
tube side of reactor diam. (m)	0.038
shell side diam. (m)	0.062
feed flow rate	0.69418

dx.doi.org/10.1021/ef300577m | *Energy Fuels* 2012, 26, 5858−5871

characteristics and input data for different sides of TCR and OTCDMR are listed in Tables 1−3.

3. REACTION SCHEME AND KINETICS

3.1. Methanol Synthesis. In the methanol synthesis, three overall reactions are as follows:[35]

Table 4. Reaction Rates and the Kinetic Parameters for Methanol Reactions

$k = A\exp(B/RT)$	A (mol·kg^{-1}·s^{-1}·bar$^{-1/2}$)	B (J·mol^{-1})
k_1	$(4.89 \pm 0.29) \times 10^7$	$-63\,000 \pm 300$
k_2	$(1.09 \pm 0.07) \times 10^5$	$-87\,500 \pm 300$
k_3	$(9.64 \pm 7.30) \times 10^6$	$-152\,900 \pm 6800$
$K = A\exp(B/RT)$	A	B (J·mol^{-1})
K_{CO}	$(2.16 \pm 0.44) \times 10^{-5}$ (bar^{-1})	$46\,800 \pm 800$
K_{CO_2}	$(7.05 \pm 1.39) \times 10^{-7}$ (bar^{-1})	$61\,700 \pm 800$
$(K_{H_2O}/K_{H_2}^{1/2})$	$(6.37 \pm 2.88) \times 10^{-9}$ (bar$^{-1/2}$)	$84\,000 \pm 1400$
$K_P = 10^{(A/T-B)}$	A (K)	B
K_{P1}	5139	12.621
K_{P2}	3066	10.592
K_{P3}	−2073	−2.029

Table 5. Parameters for Decalin Dehydrogenation Reaction

param.	value
A_{TDC}	1.54906 (kmol·kg$_{cat}^{-1}$·h^{-1})
A_{CDC}	7.89457 (kmol·kg$_{cat}^{-1}$·h^{-1})
A_{TT}	93.3959 (kmol·kg$_{cat}^{-1}$·h^{-1})
A_{NP}	2.26323 (kmol·kg$_{cat}^{-1}$·h^{-1})
A_{H2}	3.31108 (kmol·kg$_{cat}^{-1}$·h^{-1})
A_{TDC}'	221.726 (kmol·kg$_{cat}^{-1}$·h^{-1})
A_{CDC}'	40.854 (kmol·kg$_{cat}^{-1}$·h^{-1})
$A_{TDC\text{-}TT}$	363431 (kmol·kg$_{cat}^{-1}$·h^{-1})
$A_{CDC\text{-}TT}$	82710.1 (kmol·kg$_{cat}^{-1}$·h^{-1})
$A_{TT\text{-}NP}$	3357.24 (kmol·kg$_{cat}^{-1}$·h^{-1})
ΔH_{TDC}	12834.3 (J·mol^{-1})
ΔH_{CDC}	4412.80 (J·mol^{-1})
ΔH_{TT}	3888.25 (J·mol^{-1})
ΔH_{NP}	10724.7 (J·mol^{-1})
ΔH_{H}	6548.69 (J·mol^{-1})
$\Delta H_{TDC}'$	14206.2 (J·mol^{-1})
$\Delta H_{CDC}'$	6898.45 (J·mol^{-1})
$E_{TDC\text{-}TT}$	23454.7 (kJ·kmol^{-1})
$E_{CDC\text{-}TT}$	9052.43 (kJ·kmol^{-1})
$E_{TT\text{-}NP}$	7062.51 (kJ·kmol^{-1})

hydrogenation of carbon monoxide

$$CO + 2H_2 \leftrightarrow CH_3OH \quad \Delta H_{298} = -90.55\ \text{kJ/mol} \tag{1}$$

hydrogenation of carbon dioxide

$$CO_2 + 3H_2 \leftrightarrow CH_3OH + H_2O \quad \Delta H_{298} = -49.43\ \text{kJ/mol} \tag{2}$$

water−gas shift reaction

$$CO_2 + H_2 \leftrightarrow CO + H_2O \quad \Delta H_{298} = +41.12\ \text{kJ/mol} \tag{3}$$

The corresponding rate expressions for the reaction rates over commercial $CuO/ZnO/Al_2O_3$ catalysts are[36]

$$r_1^m = \frac{k_1 K_{CO}[f_{CO} f_{H_2}^{3/2} - f_{CH_3OH}/f_{H_2}^{1/2} K_{P1}]}{(1 + K_{CO} f_{CO} + K_{CO_2} f_{CO_2})[f_{H_2}^{1/2} + (K_{H_2O}/K_{H_2}^{1/2}) f_{H_2O}]} \tag{4}$$

$$r_2^m = \frac{k_2 K_{CO_2}[f_{CO_2} f_{H_2}^{3/2} - f_{CH_3OH} f_{H_2O}/f_{H_2}^{3/2} K_{P2}]}{(1 + K_{CO} f_{CO} + K_{CO_2} f_{CO_2})[f_{H_2}^{1/2} + (K_{H_2O}/K_{H_2}^{1/2}) f_{H_2O}]} \tag{5}$$

$$r_3^m = \frac{k_3 K_{CO_2}[f_{CO_2} f_{H_2} - f_{H_2O} f_{CO}/K_{P3}]}{(1 + K_{CO} f_{CO} + K_{CO_2} f_{CO_2})[f_{H_2}^{1/2} + (K_{H_2O}/K_{H_2}^{1/2}) f_{H_2O}]} \tag{6}$$

The adsorption equilibrium constants, reaction rate constants, and reaction equilibrium constants, which are used in the formulation of kinetic expressions, are tabulated in Table 4.

3.2. Decalin Dehydrogenation Reaction. The reaction scheme for the decalin dehydrogenation can be presented as follows:

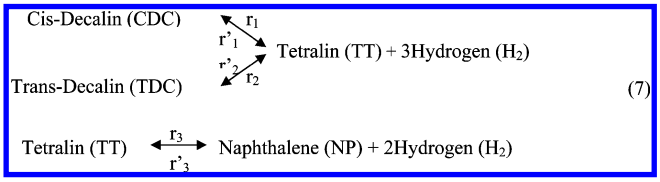

(7)

The reaction scheme shows that both *cis*-decalin and *trans*-decalin are converted into tetralin and hydrogen, and then, tetralin is dehydrogenated to naphthalene and hydrogen (final products).[15]

The dehydrogenation rates of decalin on the Pt active sites are as follows:[15]

$$r_1 = k_{r1} K_{TDC} P_{TDC}/\Delta^4 \tag{8}$$

$$r_2 = k_{r2} K_{CDC} P_{CDC}/\Delta^4 \tag{9}$$

$$r_3 = k_{r3} K_{TT} P_{TT}/\Delta^3 \tag{10}$$

$$r_1' = k_{r1}' K_{TT} K_{H_2} P_{TT} P_{H_2}{}^3/\Delta^4 \tag{11}$$

$$r_2' = k_{r2}' K_{TT} K_{H_2} P_{TT} P_{H_2}{}^3/\Delta^4 \tag{12}$$

$$r_3' = k_{r3}' K_{NP} K_{H_2} P_{NP} P_{H_2}{}^2/\Delta^3 \tag{13}$$

$$\Delta = 1 + K_{CDC} P_{CDC} + K_{TDC} P_{TDC} + K_{TT} P_{TT} + K_{H_2} P_{H_2} + K_{NP} P_{NP} \tag{14}$$

For the rate coefficient,

$$k_i = A_i \exp(-E_i/RT) \tag{15}$$

For the adsorption constant,

$$K_i = A_i \exp(-\Delta H_i/RT) \tag{16}$$

Twenty parameter estimates generated by Froment et al. are listed in Table 5.[15]

dx.doi.org/10.1021/ef300577m | Energy Fuels 2012, 26, 5858−5871

4. MATHEMATICAL MODEL

To develop the mass and energy balance equations, the one-dimensional heterogeneous model has been taken into consideration. The assumptions made during the modeling of catalytic reactors are as follows:

1. Both reactors operate in steady-state conditions.
2. The gas mixtures are assumed to be ideal.
3. The plug flow pattern is considered in each side of the reactor.
4. The reactions occur merely in the catalytic particle.
5. The decalin isomerization reaction is neglected.
6. Axial diffusion of heat and mass are neglected.
7. Heat loss is negligible.
8. Bed porosity is constant in axial and radial directions.
9. No radial heat and mass diffusion in catalyst pellet.

By using the aforementioned assumptions a differential element along the axial direction inside the reactor has been considered to achieve the energy and mole balance equations.

Table 6. Physical Properties, Mass and Heat Transfer Coefficients

param.	equation	ref
	Fixed-Bed Reactor	
component heat capacity	$C_p = a + bT + cT^2 + dT^{-2}$	
mixture heat capacity	based on local compositions	
viscosity of reaction mixtures	based on local compositions	
mixture thermal conductivity		Lindsay and Bromley[40]
mass transfer coefficient between gas and solid phases	$k_{gi} = 1.17\mathrm{Re}^{-0.42}\mathrm{Sc}_i^{-0.67}u_g \times 10^3$	Cussler[41]
	$\mathrm{Re} = \frac{2R_p u_g}{\mu}$	
	$\mathrm{Sc}_i = \frac{\mu}{\rho D_{im} \times 10^{-4}}$	
	$D_{im} = \frac{1 - y_i}{\sum_{i=j} \frac{y_i}{D_{ij}}}$	Wilke[42]
	$D_{ij} = \frac{1.43 \times 10^{-7} T^{3/2} \sqrt{1/M_i + 1/M_j}}{\sqrt{2}P(v_{ci}^{1/3} + v_{cj}^{1/3})^2}$	Reid et al.[43]
overall heat transfer coefficient	$\frac{1}{U} = \frac{1}{h_i} + \frac{A_i \ln(D_o/D_i)}{2\pi L K_w} + \frac{A_i}{A_o}\frac{1}{h_o}$	
heat transfer coefficient between gas phase and reactor wall	$\frac{h}{C_p \rho \mu}\left(\frac{C_p \mu}{K}\right)^{2/3} = \frac{0.458}{\varepsilon_B}\left(\frac{\rho u d_p}{\mu}\right)^{-0.407}$	Smith[44]

4.1. Solid Phase. The energy and mass balances for the solid phase are presented as follows:

$$a_v c_j k_{gi,j}(y^g_{i,j} - y^s_{i,j}) + \eta r_{i,j}\rho_b = 0 \tag{17}$$

$$a_v h_f(T^g_j - T^s_j) + \rho_b \sum_{i-1}^{N} \eta r_{i,j}(-\Delta H_{f,i}) = 0 \tag{18}$$

where η is the effectiveness factor. $y^s_{i,j}$ and T^s_j are the solid-phase ith-component mole fraction and temperature in jth side of reactor, respectively.

4.2. Fluid Phase. The energy and mass balances for the fluid phase in the exothermic and endothermic side of first reactor are obtained as follows:

$$-\frac{F_j}{A_{c,j}}\frac{dy^g_{i,j}}{dz} + a_v c_j k_{gi,j}(y^s_{i,j} - y^g_{i,j}) - \alpha\frac{J_{H_2O}}{A_{c,j}} - \beta\frac{J_{H_2}}{A_{c,j}} = 0 \tag{19}$$

$$-\frac{F_j}{A_{c,j}}C^g_{p_j}\frac{dT^g_j}{dz} + a_v h_f(T^s_j - T^g_j) \pm \frac{\pi D_2}{A_{c,j}}U(T^g_3 - T^g_2) - \alpha\frac{J_{H_2O}}{A_{c,j}}\int_{T_1}^{T_2} C_p dT - \beta\frac{J_{H_2}}{A_{c,j}}\int_{T_4}^{T_3} C_p dT - \alpha\frac{\pi D_1}{A_{c,j}}U_{2-1}(T^g_2 - T^g_1) - \beta\frac{\pi D_3}{A_{c,j}}U_{3-4}(T^g_3 - T^g_4) = 0 \tag{20}$$

In eq 19, α is equal to zero and $\beta = 1$ for H_2 in the endothermic side, and for H_2O in the exothermic side β is equal to zero and $\alpha = 1$. For the other components, both α and β are equal to zero. In eq 20, for the endothermic side, α is equal to zero and $\beta = 1$, and for the exothermic side, β is equal to zero and $\alpha = 1$. The positive and negative signs are used for the exothermic and endothermic sides, respectively. $y^g_{i,j}$ and T^g_j are the fluid phase mole fraction and temperature for component i in j side of reactor, respectively.

4.3. Permeation Side. The energy and mass balances for the permeation side are

H-SOD membrane:

$$-F_1\frac{dy^g_{i,1}}{dz} + \alpha J_{H_2O} = 0 \tag{21}$$

$$-F_1 C^g_{P_1}\frac{dT^g_1}{dz} + J_{H_2O}\int_{T_1}^{T_2} C_p dT + \pi D_1 U_{2-1}(T^g_2 - T^g_1) = 0 \tag{22}$$

In eq 21, for the water and N_2 in the inner side of membrane, $\alpha = 1$ and $\alpha = 0$, respectively.

Pd–Ag membrane:

$$-F_4\frac{dy^g_{i,4}}{dz} + \beta J_{H_2} = 0 \tag{23}$$

$$-F_4 C^g_{P_4}\frac{dT^g_4}{dz} + J_{H_2}\int_{T_4}^{T_3} C_p dT + \pi D_3 U_{3-4}(T^g_3 - T^g_4) = 0 \tag{24}$$

In eq 23, for the H_2 and N_2 in the outer side of membrane, $\beta = 1$ and $\beta = 0$, respectively.

4.4. Boundary Conditions. The boundary conditions applied to solve the model are as follows:

$$z = 0 \quad y^g_{i,j} = y^g_{i0,j} \quad T^g_j = T^g_{j0} \quad P^g_j = P^g_{j0} \quad j = 1, 2, 3, 4 \tag{25}$$

$y^g_{i0,j}$, T^g_0, and P^g_0 are the fluid-phase mole fraction, temperature, and pressure at the entrance of the jth side of the reactor, respectively.

4.5. Water Permeation Through H-SOD Membrane. Water permeation flux in H-SOD membrane is presented as follows:

$$J_{H_2O} = \frac{A_s}{V_r}Q_{H_2O}(P_{H_2O}{}^2 - P_{H_2O}{}^1) \tag{26}$$

dx.doi.org/10.1021/ef300577m | Energy Fuels 2012, 26, 5858–5871

where Q_{H_2O} is water permeation, which is a membrane property and depends on temperature.[25] As seen in eq 26, J_{H_2O} depends upon the water partial pressure difference between two sides of the membrane.

4.6. Hydrogen Permeation in Pd−Ag Membrane. In this study, a composite membrane that is made of a thin layer of palladium−silver alloy is used. The hydrogen permeation flux in the Pd−Ag membrane is assumed as follows:

$$J_{H_2} = A_0 \exp\left(\frac{-E_a}{RT}\right) \times \left(\sqrt{P_{H_2}}^{3} - \sqrt{P_{H_2}}^{4}\right)$$
$$E_a = 29.16\ [\mathrm{kJ/mol}]$$
$$\mathrm{Pe}_0 = 1.12 \times 10^{-5}\ [\mathrm{mol \cdot m/(s \cdot m^2 \cdot Pa^{0.5})}]$$
$$A_0 = \mathrm{Pe}_0/\delta \tag{27}$$

where δ is the membrane thickness.[37]

4.7. Pressure Drop. Ergun momentum balance equation has been used to calculate the pressure drop in the reactor:

$$\frac{dP}{dz} = 150\frac{(1-\varepsilon)^2 \mu u_g}{\varepsilon^3 d_p^2} + 1.75\frac{(1-\varepsilon) u_g^2 \rho}{\varepsilon^3 d_p} \tag{28}$$

where the pressure drop is in Pa.

4.8. Auxiliary Correlations. Auxiliary correlations should be used for the purpose of reactor simulation in the heterogeneous model. The heat and mass transfer between solid and fluid phase should be considered owing to the transfer phenomena. Physical properties of the components are necessary for the simulation procedure. Table 6 lists the correlations for physical properties and mass and heat coefficients.

5. DIFFERENTIAL EVOLUTION (DE) METHOD

Differential evolution is a technique based on random search methods and optimization evolutionary algorithms. This method has been proposed by Price and Storn[38] for the first time. It is because of its properties, such as being a fast and robust method in numerical optimization, simplicity of its use, and its ability to find a function's true global optimum, that the DE method can be used for minimizing of nonlinear, multimodal, differentiable, and optimization problems that involve complex mathematical models.[31] By utilizing DE, the minimum number of input data is required. The main input variables include NP (number of populations), F (scaling factor) and CR (cross over constant). Choosing NP, F and CR is often difficult and depends upon the problem that is applied. By use of some general guidelines, usually, NP should be about 5−10 times the number of parameters in a vector, F lies in the range 0.4−1, and a first choice for CR can be 0.1, but generally, CR should be as large as possible.[32] More details about the DE-based version, its various strategies, and choosing the operating parameters can be found in previous publications.[31,39] The strategy and parameters that are used in this work are presented in Table 7. In this study, maximizing the methanol yield in the first-reactor exothermic side, the hydrogen yield in the endothermic side and decalin yield in the second reactor is the optimization goal. Methanol is the major product. When the rate of hydrogen extraction from endothermic side increases, more decalin is consumed. Consequently, more methanol can be achieved due to higher heat transfer. Also, to produce more decalin and enhance the volume of stored decalin, the yield of output decalin is inserted into the objective function. Four decision variables that have more effect on the production rates are as follows: T_{02}^{1}, the inlet temperature of the first-reactor exothermic side, T_{03}^{1}, the inlet temperature of the first-reactor endothermic side, T_s^2, the temperature of shell side of the second reactor and, L^2, the length of the second reactor. To validate the OTCDMR, the initial molar flow rate of first-reactor exothermic side is considered equal to molar flow rate of conventional methanol synthesis reactor and is not selected as a decision variable. The temperature of tubular reactors is a key parameter due to its direct effect on the reaction rate, catalyst activity, and thermodynamic equilibrium. Because of the great effect of inlet temperature on production rates, it is selected as a decision variable. The second-reactor shell side temperature controls the thermodynamic equilibrium. Thus, like the second-reactor length, it has a great effect on the decalin production. To ensure that the temperature of inlet synthesis gas is not too low for methanol synthesis to occur or not too high that catalyst may be deactivated, lower and upper bounds are needed. The lower bound is set at 495 K, and the upper bound of 535 K is chosen for exothermic side inlet temperature.[45] The temperature of decalin dehydrogenation is in the range 483−553 K.[15] The second reactor shell side temperature range is equivalent to naphthalene hydrogenation reaction temperature range. The length of the second reactor is optimized and 3 m is selected as the most economical one (ranges between 1 and 5 is considered during the optimization process). In order to make a driving force for heat transfer through the solid wall, the exothermic side temperature should be higher than that of the endothermic side. The objective function, the range of decision variables and the constrains are defined as follows:

$$F = Y_{CH_3OH}^{1} + Y_{H_2}^{1} + Y_{decalin}^{2} \tag{29}$$

where

$$\text{methanol yield} = \frac{F_{CH_3OH}^{\text{outlet}}}{F_{CO}^{\text{inlet}} + F_{CO_2}^{\text{inlet}}} \tag{30}$$

$$\text{hydrogen yield} = \frac{F_{H_2}^{\text{outlet}}}{F_{decalin}^{\text{inlet}}} \tag{31}$$

where

Table 7. Strategy and Parameters Used for DE Method

param. (abbrev.)	value
population size (NP)	30
scaling factor (F)	0.8
cross over constant (CR)	1.0

Table 8. Optimization Results

param. (unit)	value
inlet temp. of exothermic side (K)	505.1
inlet temp. of endothermic side (K)	502
temp. of the shell side in the second reactor (K)	504
length of the second reactor (m)	3

dx.doi.org/10.1021/ef300577m | Energy Fuels 2012, 26, 5858−5871

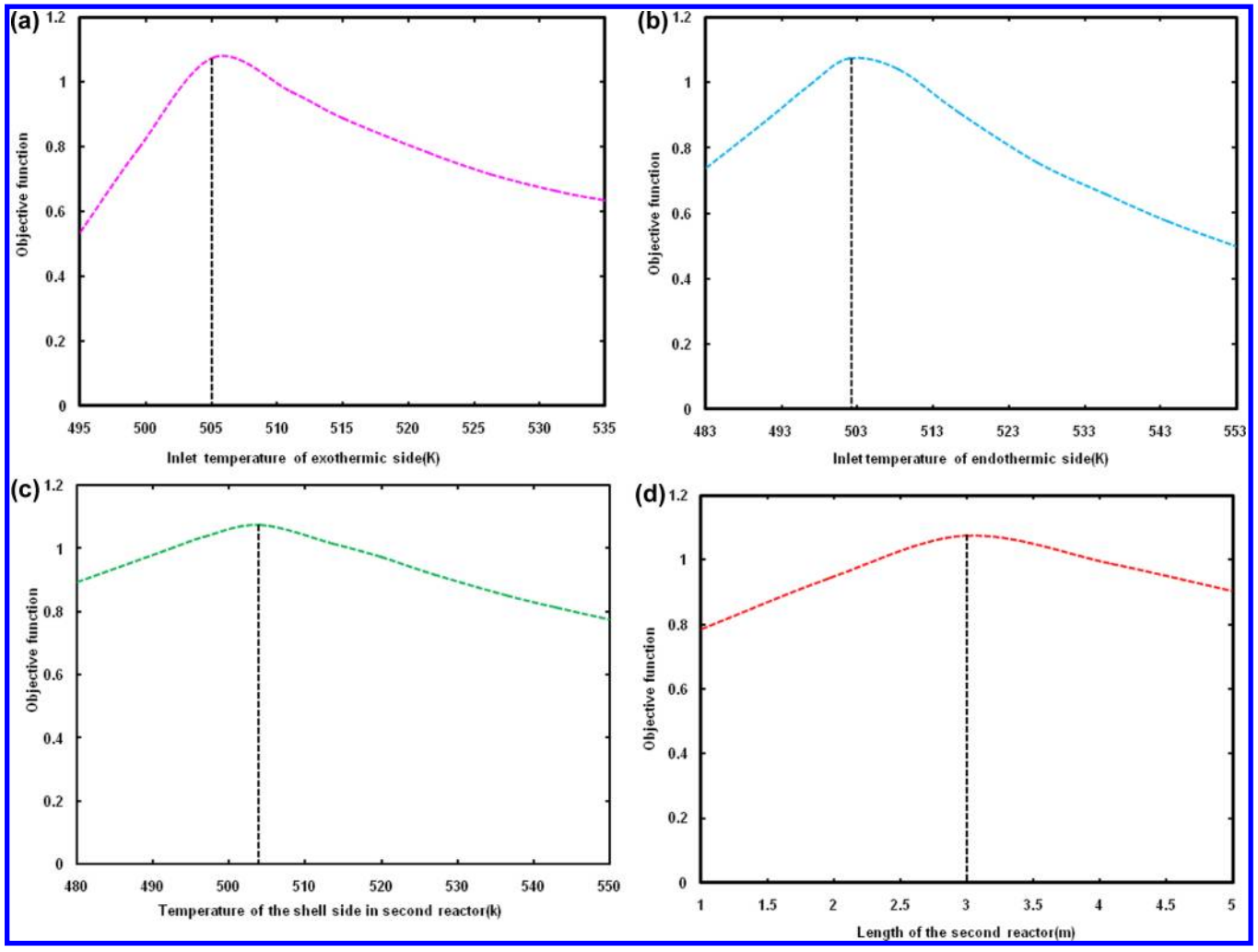

Figure 2. Profiles of the objective function in terms of inlet temperature of exothermic (a) and endothermic (b) sides, the shell side temperature (c), and the length of second rector (d) in OTCDMR.

$$F_{H_2}^{\text{outlet}} = F_{H_2}^{\text{outlet,membrane side}} + F_{H_2}^{\text{outlet,endothermic side}}$$

$$\text{decalin yield} = \frac{F_{\text{decalin}}^{\text{outlet}}}{F_{H_2}^{\text{inlet}} + F_{Np}^{\text{inlet}}} \tag{32}$$

The range of decision variable

$$495 < T_{02}^{1} < 535 \text{ K} \tag{33}$$

$$483 < T_{03}^{1} < 553 \text{ K} \tag{34}$$

$$480 < T_{S}^{2} < 550 \text{ K} \tag{35}$$

$$1 < L^{2} < 5 \text{ m} \tag{36}$$

The constrains

$$495 < T_{2}^{1} < 535 \text{ K} \tag{37}$$

$$483 < T_{3}^{1} < 553 \text{ K} \tag{38}$$

$$T_{2}^{1} > T_{3}^{1} \tag{39}$$

$$480 < T_{s}^{2} < 550 \text{ K} \tag{40}$$

In this study, the penalty function method has been used for handling constraints and 10^7 is used as a penalty parameter, but this parameter can vary with problems owing to its dependence on the order of the magnitude of the decision variables. The objective function (OF), which should be minimized, in conclusion, is

$$\text{OF} = -F + 10^7 \sum_{i=1}^{10} G_i^2 \tag{41}$$

where

$$G_1 = \max(0, (T_2^1 - 535)) \tag{42}$$

$$G_2 = \max(0, (495 - T_2^1)) \tag{43}$$

$$G_3 = \max(0, (T_3^1 - 553)) \tag{44}$$

$$G_4 = \max(0, (483 - T_3^1)) \tag{45}$$

$$G_5 = \max(0, (T_3^1 - T_2^1)) \tag{46}$$

$$G_6 = \max(0, (T_s^2 - 550)) \tag{47}$$

$$G_7 = \max(0, (480 - T_s^2)) \tag{48}$$

dx.doi.org/10.1021/ef300577m | *Energy Fuels* 2012, 26, 5858−5871

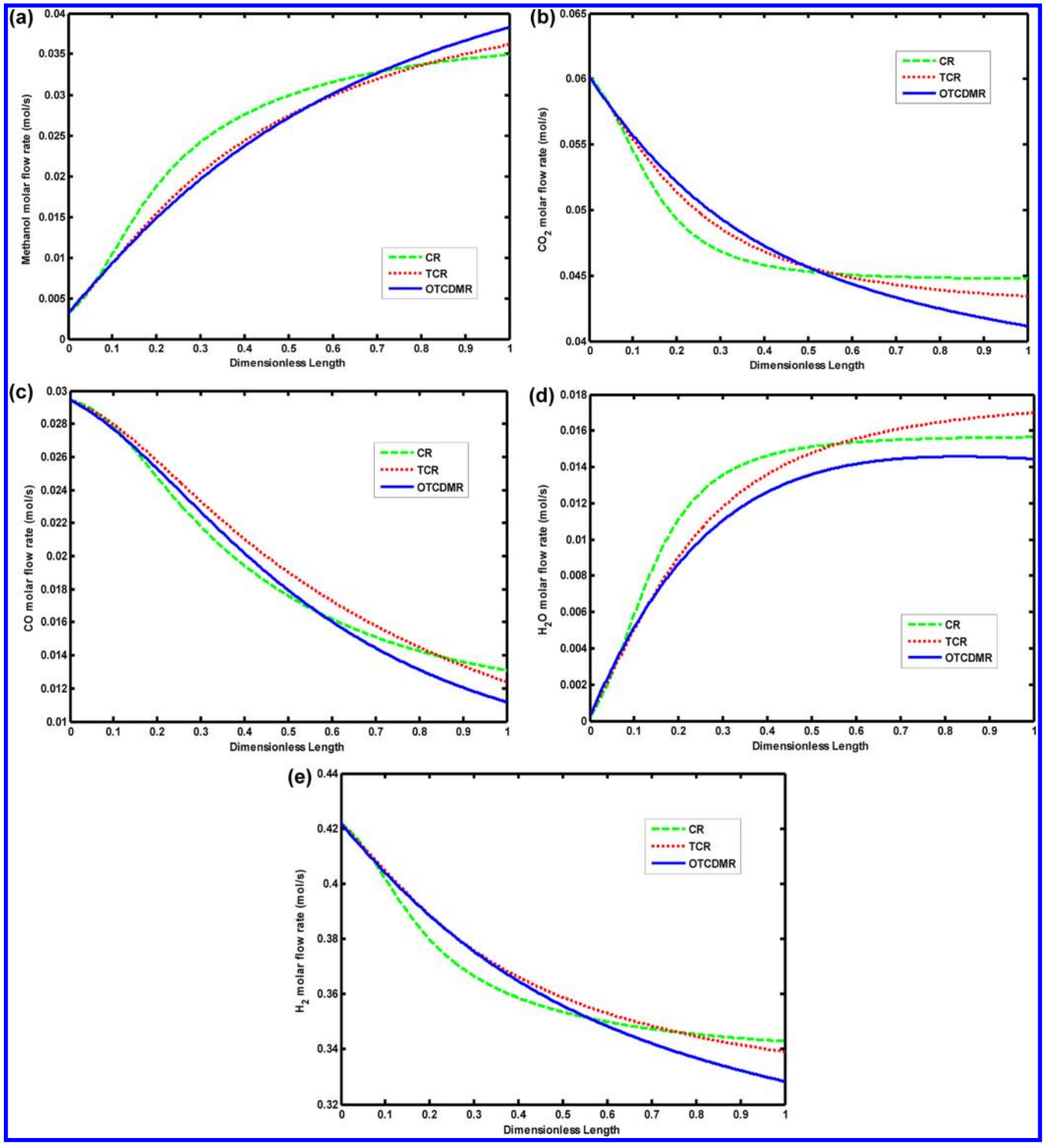

Figure 3. (a) Methanol, (b) carbon dioxide, (c) carbon monoxide, (d) water, and (e) hydrogen molar flow rate profiles in OTCDMR, TCR, and CR.

$$G_8 = \max(0, (L^2 - 5)) \tag{49}$$

$$G_9 = \max(0, (1 - L^2)) \tag{50}$$

The DE algorithm is used to solve the resulting optimization problems. These equations are coupled with nonlinear algebraic equations of the kinetic model, transport property correlations, and other auxiliary correlations. A backward finite difference approximation method is used to solve the set of equations. The optimized result is listed in Table 8.

6. RESULTS AND DISCUSSION

In this section, the profiles of objective function, the molar flow rates, mole fractions, conversions, and temperature profiles of the reactants and products are depicted and compared in the following figures. Figure 2a–d shows the profiles of the objective function in terms of inlet temperature of exothermic and endothermic sides, the shell side temperature and the length of second rector in OTCDMR, respectively. In each figure, three of four decision variables are set on the optimized result and as the fourth one changes, the maximum of the

dx.doi.org/10.1021/ef300577m | *Energy Fuels* 2012, 26, 5858–5871

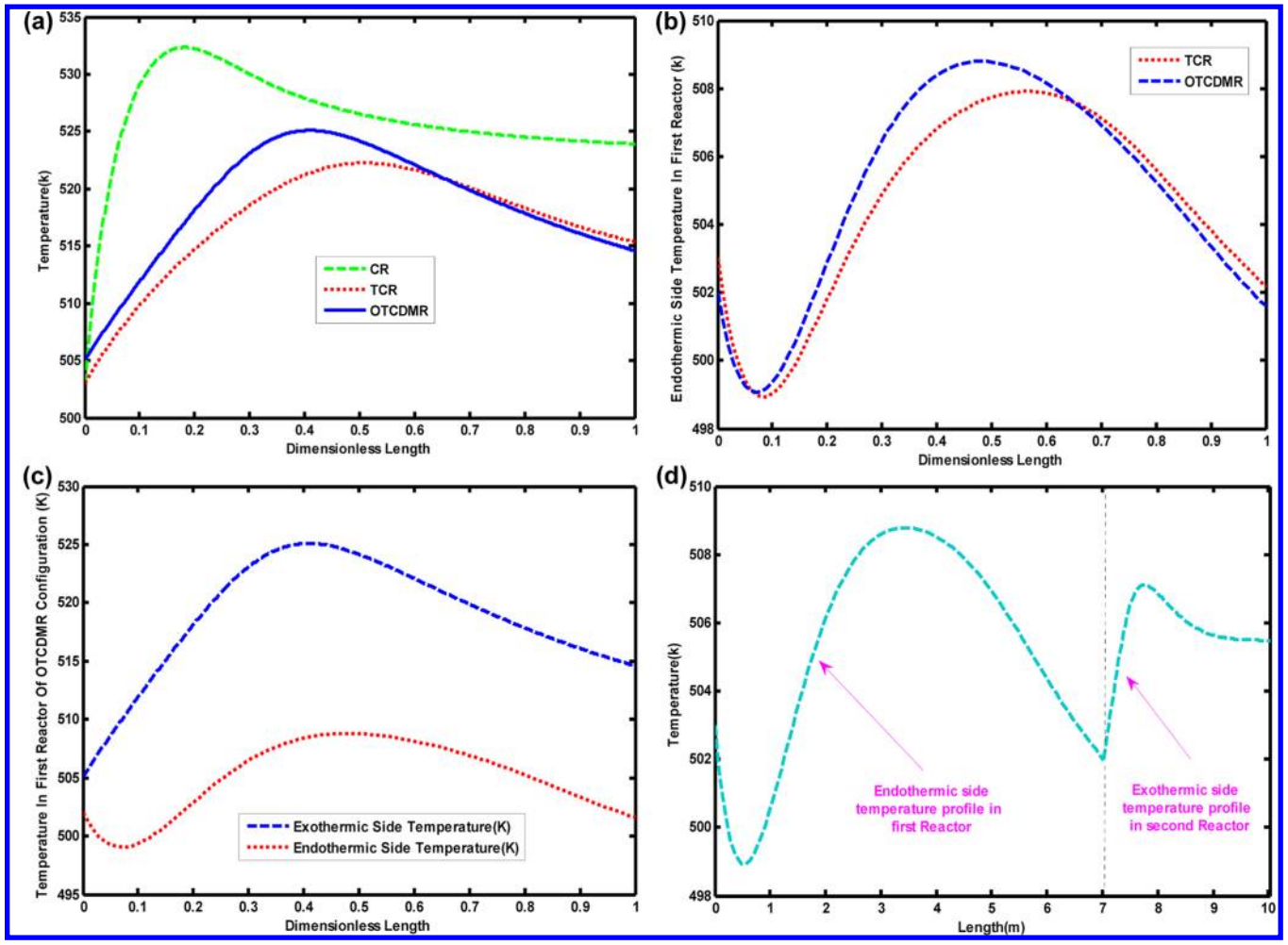

Figure 4. Variation of temperature profiles along the reactors.

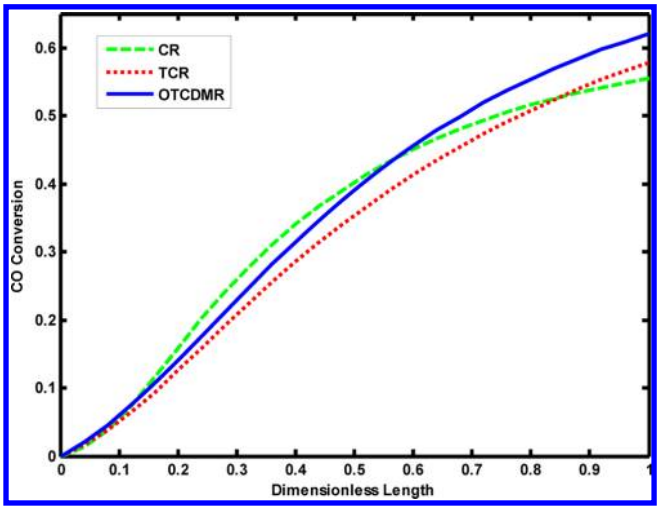

Figure 5. Comparison between CO conversion in CR and the exothermic side of OTCDMR and TCR.

objective function is achieved in the optimized value of the fourth decision variable. This means there is an optimal inlet temperature of exothermic and endothermic sides, an optimal length of second reactor and an optimal shell side temperature and their values are 505.1 K, 502 K, 3 m, and 504 K, respectively.

Figure 3a shows the methanol molar flow rate profile in all the three configurations (OTCDMR, TCR, and CR). As can be seen, OTCDMR and TCR configurations provide better results than the conventional reactor for methanol production. The endothermic reaction from the shell side of coupled reactors decreases the exothermic side temperature, thereby delaying the thermodynamic equilibrium, and therefore, the reaction shifts toward the products (methanol, etc.). The difference between the outputs of OTCDMR and TCR is mainly due to the water removal from the exothermic side and the H_2 extraction from endothermic side of OTCDMR. As a result of the water removal, the methanol reaction yield will increase, and higher methanol can be obtained. Moreover, the H_2 extraction from the OTCDMR endothermic side enhances the yield of naphthalene production reaction. Hence, much more heat is transferred from the methanol production side, and further methanol is produced. The CO_2 molar flow rate is shown in Figure 3b. The CO_2 consumption rate in OTCDMR is greater than that of TCR and in TCR is greater than that of CR owing to the difference in the methanol production rate. Since the methanol reactions consume CO_2, each configuration that produces more methanol needs more CO_2. CO_2 is consumed owing to the in situ water removal (via H-SOD membrane layer), which shifts the methanol reactions to the product sides in OTCDMR. Therefore, the minimum molar flow rate of CO_2 is seen in OTCDMR configuration. Figure 3c shows similar results for CO component. Higher heat transfer

dx.doi.org/10.1021/ef300577m | Energy Fuels 2012, 26, 5858−5871

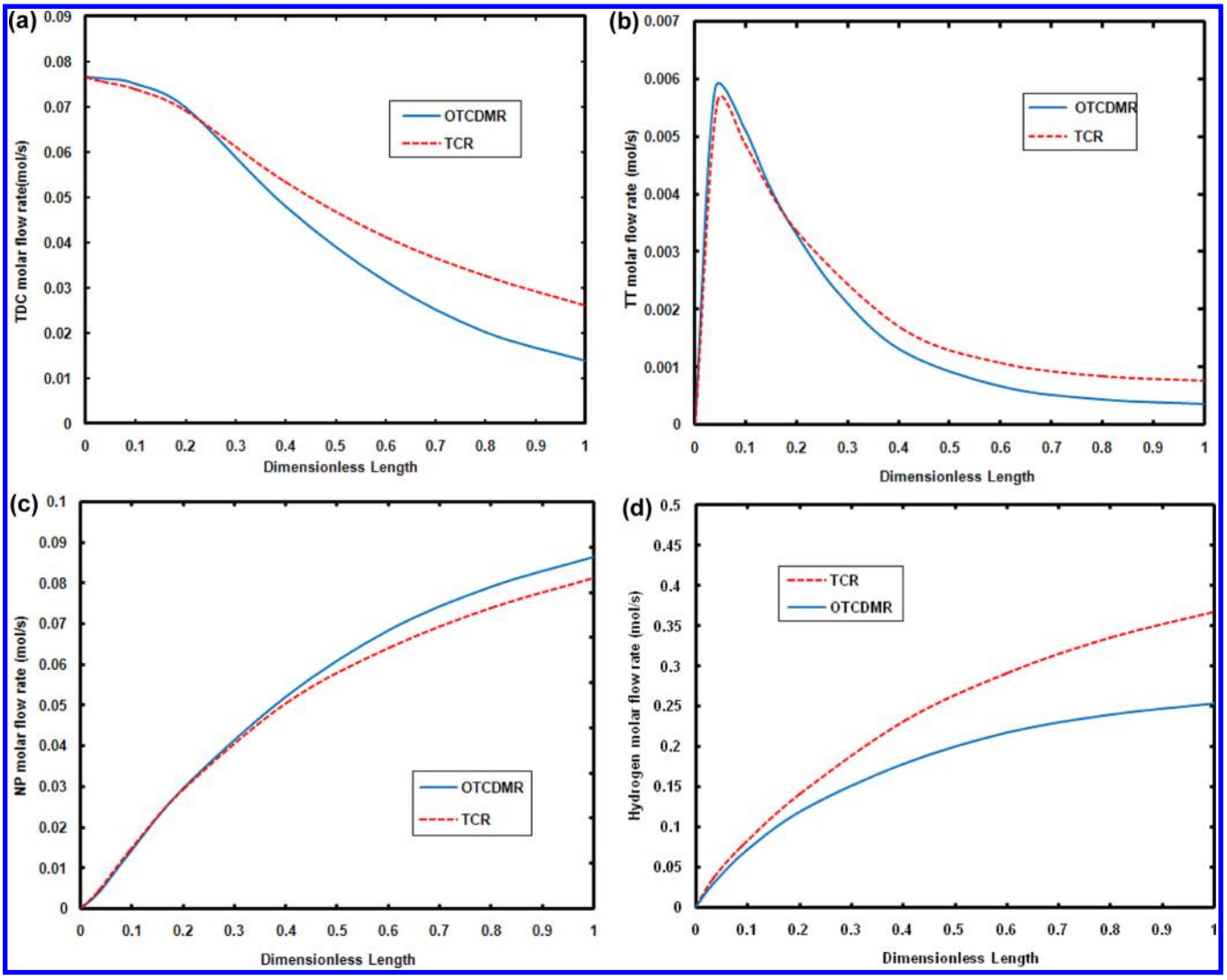

Figure 6. Molar flow rate of the endothermic side components in the coupled configurations.

in the coupled configurations yields more methanol production, and as a consequence, the CO consumption rate increases. Figure 3d demonstrates the H_2O molar flow rate profile. Coupled reactors produce more H_2O in comparison with CR due to the higher reaction yield, but the OTCDMR output is the lowest due to the use of the H-SOD membrane to remove water from reaction side. Figure 3e presents the H_2 molar flow rate profiles for all configurations. The delay in the thermodynamic equilibrium caused by coupling the endothermic and exothermic reactions, leads to an increase in the methanol production rate and the CO, CO_2, H_2 consumption rates in OTCDMR and TCR. Therefore, the maximum H_2 is seen in the CR. The H_2 molar flow rate in OTCDMR is less than that of TCR, mainly owing to the application of membrane layers in OTCDMR.

The variations of temperature profile along the reactors are depicted in Figure 4. Figure 4a presents the temperature profiles of the conventional reactor and exothermic side of TCR and first reactor in OTCDMR. As can be observed in this figure, for all the three configurations, temperature increases rapidly along the reactor, a hot spot appears, and afterward, it decreases. In the initial section of the reactor, a great amount of heat is generated due to the high methanol reaction rate, but it does not have a sufficient time to be transferred. Consequently, the temperature rises sharply. Afterward, as the reaction proceeds, the reaction rate decreases due to the fact that the reaction shifts toward the equilibrium. Thus, the figure shows the downward trend of temperature. The exothermic side temperature profiles of OTCDMR and TCR lie in a lower position as compared with CR because of using an endothermic reaction in the shell side of the coupled reactors. Figure 4a also compares the OTCDMR first-reactor and TCR exothermic side temperature profiles. The exothermic reaction rate at the entrance of OTCDMR is higher than that of TCR. Thus, OTCDMR has a higher temperature owing to the higher heat generation quantity. In the final section of the reactor, because of the higher endothermic reaction rate, OTCDMR has a lower temperature in comparison with TCR. The reaction rate of OTCDMR endothermic side is higher than that of TCR, mainly owing to H_2 extraction from the endothermic side of OTCDMR. Figure 4b compares the endothermic side temperature of the coupled reactors. Both reactors have a similar trend. At the entrance of the reactors, the plot shows a decreasing trend due to the fact that sufficient heat cannot be provided for the endothermic side by the exothermic side and the shell side reaction does not proceed properly. Afterward, the reaction rate is enhanced owing to the increasing heat transfer. Hence, the figure shows an increasing trend. At the

dx.doi.org/10.1021/ef300577m | *Energy Fuels* 2012, 26, 5858−5871

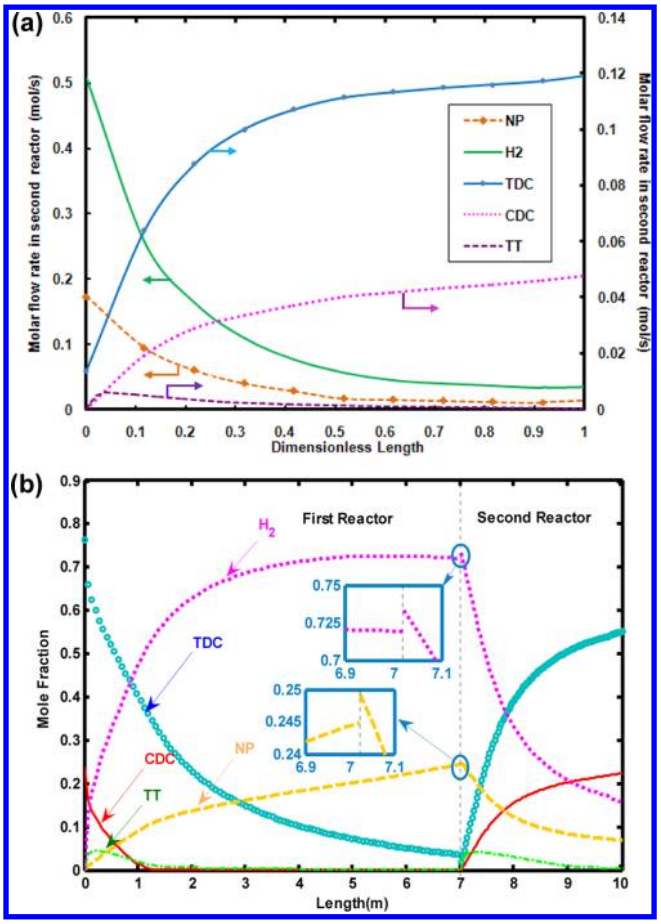

Figure 7. (a) Molar flow rate profile of the exothermic side of second reactor. (b) Mole fraction profile of the first reactor endothermic side and second reactor exothermic side.

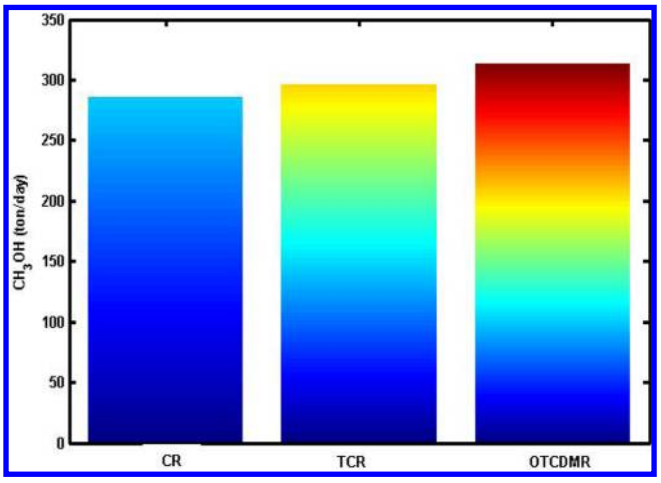

Figure 8. Methanol production in OTCDMR, TCR, and CR.

end of the reactors, the exothermic reaction goes toward the equilibrium. Thus, the reaction rate and the generated heat decrease, leading to a decrease in temperature in both sides. At the first part of the plot, OTCDMR has a lower position as compared with TCR due to the higher reaction rate of endothermic side. Afterward, OTCDMR has a higher position due to the higher exothermic side temperature, and then the lower exothermic side temperature in OTCDMR leads to a lower temperature in the endothermic side. The next figure

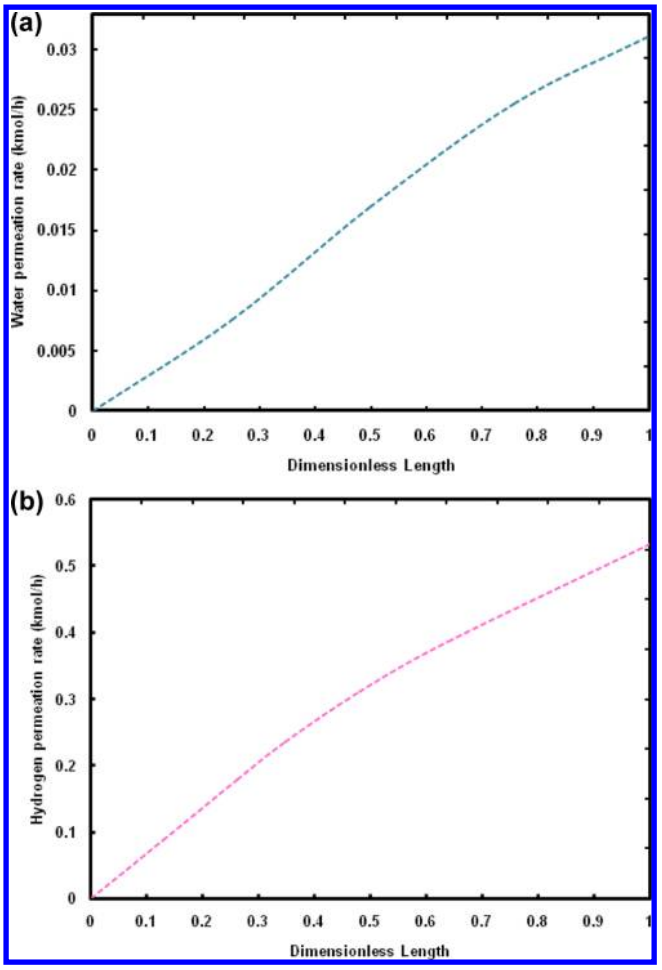

Figure 9. Water (a) and hydrogen (b) permeation from the membrane sides.

(Figure 4c) shows the OTCDMR first-reactor temperature profile in both sides. As seen, the temperature profile of the endothermic side always lies under that of the exothermic side as a driving force is needed to transfer the heat. The simultaneous temperature profiles of decalin consumption and production reactions in the first and second reactors in OTCDMR configuration are shown in Figure 4d. At the entrance of first-reactor shell side, the temperature decreases rapidly because of the low heat transfer and the high reaction rate of endothermic side. Then, it increases due to an increase in heat transfer. afterward, it decreases because when the exothermic side temperature reduces owing to the approaching equilibrium, the reaction takes place slowly. In the second reactor in the OTCDMR configuration, at first, the reaction progress is rapid and an increase in temperature appears, and then, the temperature decreases due to the heat exchange with the cooling water.

Figure 5 presents a comparison between CO conversions in CR and the exothermic side of OTCDMR and TCR. As seen in this figure, the CO conversion in OTCDMR and TCR are higher than CR due to the variation of temperature in the shell side. The lower temperature in the shell side of coupled reactor owing to the presence of endothermic reaction leads to a thermodynamic equilibrium delay and shifts the reaction toward the higher production quantity. The higher position of OTCDMR conversions in comparison with TCR in the figure is logical because of the application of membranes.

dx.doi.org/10.1021/ef300577m | *Energy Fuels* 2012, 26, 5858−5871

The molar flow rates of the endothermic side components in the OTCDMR first-reactor and TCR are depicted in Figure 6. Figure 6a shows the TDC molar flow rate profile in the two configurations (OTCDMR and TCR). By water removal from the exothermic side, by hydrogen extraction from the endothermic side of the first reactor and by applying optimized operating conditions in OTCDMR, the naphthalene production reaction is shifted to the consumption of more TDC in comparison with TCR. The tetralin molar flow rate profile in OTCDMR and TCR is shown in Figure 6b. TT (tetralin) is produced at the entrance of the reactor and then utilized (naphthalene is the consumer of tetralin). In other words, TT is an intermediate product. As can be observed in the Figure 6b, at first, the TT molar flow rate increases progressively and then decreases, and at the end of the reactor, it approximates to zero. In the first part of the plot, it can be seen that TT production in OTCDMR is higher than that of TCR because of the higher yield of TT production reaction in OTCDMR. Afterward, the naphthalene reaction goes up, and as a consequence, TT consumption becomes higher. The TT consumption quantity in TCR is lower than that of OTCDMR owing to its lower reaction yield. Hence, in the second half of the reactor, the plot of OTCDMR is placed under the plot of TCR. The naphthalene molar flow rate profile in OTCDMR and TCR is depicted in Figure 6c. The produced naphthalene molar flow rate in OTCDMR is more than the one in TCR. Based upon the reasons mentioned in the preceding parts, OTCDMR has a higher reaction yield quantity. Therefore, decalin consumption increases and more naphthalene is produced. Figure 6d shows the H_2 molar flow rate, which is lower in OTCDMR as against TCR; however, H_2 production in OTCDMR is higher than that of TCR, but due to using a membrane in OTCDMR, some hydrogen is extracted.

The second reactor molar flow rate profile in OTCDMR is shown in Figure 7a. This figure shows that all of H_2 is not consumed, and its molar flow rate does not approach zero. Hence, the unreacted hydrogen is sent back to the feed of the second reactor. The mole fractions of all endothermic components of the first reactor and the exothermic-side components of the second reactor are shown in Figure 7b simultaneously. It is worth mentioning that the naphthalene mole fraction at the entrance of the second reactor is in a higher position than the exit of the first reactor because at the entrance of the second reactor due to the naphthalene input stream from other sources, the naphthalene mole fraction is the highest.

Figure 8 illustrates the methanol production in each configuration. The methanol production of OTCDMR is 17 and 28 t·day^{-1} higher than TCR and CR, respectively.

The water and hydrogen permeation from the membrane sides are depicted in Figure 9. The permeation quantities along the reactor show an increasing trend owing to an increase in the pressure difference between the membrane side and the reaction side. Along the reactor, as the reaction proceeds, more water and hydrogen are produced. Therefore, the pressure deference between the reaction side and the permeation side enhances.

7. CONCLUSION

In this work, a new configuration is recommended for producing and utilizing decalin and hydrogen simultaneously. The new configuration is made up of two reactors. In the first reactor, methanol synthesis occurs in the tube side and supplies the heat needed for the shell side (decalin dehydrogenation). The Pd−Ag and H-SOD membrane layers are applied in the first reactor. The Pd−Ag membrane layer extracts hydrogen from decalin dehydrogenation region to enhance the naphthalene production and the H-SOD membrane layer increase methanol production by removing water from the first-reactor tube side. The produced naphthalene from the first reactor enters the second reactor to be utilized as some portion of required naphthalene. Some amount of exit decalin from the second reactor is introduced as an inlet feed for the first reactor and the other part is stored. To obtain a higher amount of valuable products, DE method is used to optimize operating conditions of this configuration. Four decision variables, such as the inlet temperature of both exothermic and endothermic sides of first reactor, the inlet shell side temperature, and the length of the second reactor, are taken into account. As the results show, the OTCDMR configuration produces further methanol in comparison with TCR and CR (OTCDMR methanol production is 17 and 28 t·day^{-1} higher than that of TCR and CR, respectively), mainly owing to the use of membranes and applying optimized operating conditions. Also, this configuration has a lower temperature in comparison with CR, which can decrease the deactivation rate of catalyst. Another superiority of OTCDMR is its use of decalin as an energy carrier and hydrogen storage to resolve the hydrogen storage problem. These advantages clearly show that optimized thermally coupled dual methanol reactor could be beneficial.

AUTHOR INFORMATION

Corresponding Author

*Tel: +98 711 2303071. Fax: +98 711 6287294. E-mail: rahimpor@shirazu.ac.ir.

Notes

The authors declare no competing financial interest.

NOMENCLATURE

C_p = specific heat of the gas at constant pressure, J·mol^{-1}·K^{-1}
d_p = particle diameter, m
D_i = inside diameter, m
D_{ij} = binary diffusion coefficient of component i in j, m^2·s^{-1}
D_{im} = diffusion coefficient of component i in the mixture, m^2·s^{-1}
D_o = outside diameter, m
E_i = activation energy for elementary reaction step i, kg·kmol^{-1}
f_i = partial fugacity of component i, bar
F = total molar flow rate, mol·s^{-1}
h_f = gas−solid heat transfer coefficient, W·m^{-2}·K^{-1}
h_i = heat transfer coefficient between fluid phase and reactor wall in exothermic side, W·m^{-2}·K^{-1}
h_o = heat transfer coefficient between fluid phase and reactor wall in endothermic side, W·m^{-2}·K^{-1}
ΔH_{fi} = enthalpy of formation of component i, J·mol^{-1}
J_{H_2} = permeation rate of hydrogen through the Pd−Ag membrane, mol·s^{-1}
k_1 = rate constant for the first rate equation of methanol synthesis reaction, mol·kg^{-1}·s^{-1}·bar$^{-1/2}$
k_2 = rate constant for the second rate equation of methanol synthesis reaction, mol·kg^{-1}·s^{-1}·bar$^{-1/2}$
k_3 = rate constant for the third rate equation of methanol synthesis reaction, mol·kg^{-1}·s^{-1}·bar$^{-1/2}$
k_i = reaction rate coefficient, kmol·kgcat^{-1}·h^{-1}
k_{gi} = mass transfer coefficient for component i, m·s^{-1}

dx.doi.org/10.1021/ef300577m | Energy Fuels 2012, 26, 5858−5871

K = conductivity of gas phase, $W \cdot m^{-1} \cdot K^{-1}$
K_i = adsorption equilibrium constant, bar^{-1}
K_{pi} = equilibrium constant based on partial pressure for component i in methanol synthesis reaction
K_w = thermal conductivity of reactor wall, $W \cdot m^{-1} \cdot K^{-1}$
L = reactor length, m
M_i = molecular weight of component i, $g \cdot mol^{-1}$
P = total pressure, bar
P_i = partial pressure of component i, Pa
$P^1_{H_2O}$ = partial pressure of water in inner permeation side, Pa
$P^2_{H_2O}$ = partial pressure of water in exothermic side, Pa
Q = permeance of components, $mol \cdot s^{-1} \cdot m^{-2} \cdot Pa^{-1}$
r^m_1 = rate of reaction for hydrogenation of CO, $mol \cdot kg^{-1} \cdot s^{-1}$
r^m_2 = rate of reaction for hydrogenation of CO_2, $mol \cdot kg^{-1} \cdot s^{-1}$
r^m_3 = rate of reversed water−gas shift reaction, $mol \cdot kg^{-1} \cdot s^{-1}$
R = universal gas constant, $J \cdot mol^{-1} \cdot K^{-1}$
r_i = reaction rate of component i, $mol \cdot kg^{-1} \cdot s^{-1}$
Re = Reynolds number
Sc_i = Schmidt number of component i
T = temperature, K
u = superficial velocity of fluid phase, $m \cdot s^{-1}$
u_g = linear velocity of fluid phase, $m \cdot s^{-1}$
U = overall heat transfer coefficient between exothermic and endothermic sides, $W \cdot m^{-2} \cdot K^{-1}$
v_{ci} = critical volume of component i, $cm^3 \cdot mol^{-1}$
X_i = conversion of component i
y_i = mole fraction of component i, $mol \cdot mol^{-1}$
y^s_i = mole fraction of component i in solid phase
y^g_i = mole fraction of component i in gas phase
z = axial reactor coordinate, m

Greek Letters

ΔH_{fi} = enthalpy of formation of component i, $J \cdot mol^{-1}$
ΔH_i = enthalpy of reaction
ΔH_{298} = enthalpy of reaction at 298 K, $J \cdot mol^{-1}$
ε_B = void fraction of catalytic bed
μ = viscosity of fluid phase, $kg \cdot m^{-1} \cdot s^{-1}$
ν_{ci} = critical volume of component i, $cm^3 \cdot mol^{-1}$
ρ = density of fluid phase, $kg \cdot m^{-3}$
ρ_b = density of catalytic bed, $kg \cdot m^{-3}$
η = catalyst effectiveness factor

Superscript

g = in bulk gas phase
s = at the surface of the catalyst

Subscript

0 = inlet conditions
i = chemical species
j = reactor sides (1, inner permeation side; 2, exothermic side; 3, endothermic side; 4, outer permeation side)

Abbreviations

CDC = *cis*-decalin
TDC = *trans*-decalin
NP = naphthalene or number of populations
TT = tetralin

■ REFERENCES

(1) Ball, M.; Wietschel, M. *Int. J. Hydrogen Energy* **2009**, *34*, 615−627.
(2) Steur, K.; Bildea, C. S.; Altimari, P.; Dimian, A. C. *Comput. Chem. Eng.* **2009**, *33*, 628−635.
(3) Ramaswamy, R. C.; Ramachandran, P. A.; Dudukovíc, M. P. *Chem. Eng. Sci.* **2006**, *61*, 459−472.
(4) Ramaswamy, R. C.; Ramachandran, P. A.; Dudukovíc, M. P. *Chem. Eng. Sci.* **2008**, *63*, 1654−1667.
(5) van Sint Annaland, M.; Nijssen, R. C. *Chem. Eng. Sci.* **2002**, *57*, 4967−4985.
(6) Wang, L.; Yang, L.; Zhang, Y.; Ding, W.; Chen, S.; Fang, W.; Yang, Y. *Fuel Process. Technol.* **2010**, *91*, 723−728.
(7) Manenti, F.; Cieri, S.; Restelli, M. *Chem. Eng. Sci.* **2011**, *66*, 152−162.
(8) Rahimpour, M. R.; Ghader, S. *Chem. Eng. Process.* **2004**, *43*, 1181−1188.
(9) Khademi, M. H.; Rahimpour, M. R.; Jahanmiri, A. *Int. J. Hydrogen Energy* **2010**, *35*, 1936−1950.
(10) Rahimpour, M. R.; Lotfinejad, M. *Chem. Eng. Process.* **2008**, *47*, 1819−1830.
(11) Hodoshima, S.; Shono, A.; Saito, Y. *Energy Fuels* **2008**, *2*, 2559−2569.
(12) Sebastián, D.; Bordejé, E. G.; Calvillo, L.; Lázaro, M. J.; Moliner, R. *Int. J. Hydrogen Energy* **2008**, *33*, 1329−1334.
(13) Cooper, A. C.; Bagzis, L. D.; Campbell, K. M.; Pez, G. P. *Prepr. Symp. Am. Chem. Soc. Div. Fuel Chem.* **2005**, *50* (1), 271−273.
(14) Hodoshima, S.; Arai, H.; Takaiwa, S.; Saito, Y. *Int. J. Hydrogen Energy* **2003**, *28*, 1255−1262.
(15) Wang, B.; Wayne Goodman, D.; Froment, G. F. *J. Catal.* **2008**, *253*, 229−238.
(16) Iranshahi, D.; Pourazadi, E.; Paymooni, K.; Rahimpour, M. R. *AIChE J.* DOI: 10.1002/aic.12664.
(17) Wieland, I. S.; Melin, I. T.; Lamm, I. A. *Chem. Eng. Sci.* **2002**, *57*, 1571−1576.
(18) Unruh, D.; Rohde, M. P.; Schaub, G. *Stud. Surf. Sci. Catal.* **2004**, *153*, 91.
(19) Nam, S. E.; Lee, K. H. *J. Membr. Sci.* **2001**, *192*, 177−185.
(20) Okazaki, J.; Tanaka, D. A. P.; Tanco, M. A. L.; Wakui, Y.; Mizukami, F.; Suzuki, T. M. *J. Membr. Sci.* **2006**, *282*, 370−374.
(21) Iranshahi, D.; Pourazadi, E.; Paymooni, K.; Jahanmiri, A.; Rahimpour, M. R. *Chem. Eng. J.* **2011**, *178*, 264−275.
(22) Iranshahi, D.; Pourazadi, E.; Paymooni, K.; Rahimpour, M. R. *Chem. Eng. Sci.* **2012**, *68*, 236−249.
(23) Breck, D. W. *Zeolite Molecular Sieves*; JohnWiley: New York, 1974.
(24) Khajavi, S.; Jansen, J. C.; Kapteijn, F. *Catal. Today* **2010**, *156*, 132−139.
(25) Rohde, M. P.; Schaub, G.; Khajavi, S.; Jansen, J. C.; Kapteijn, F. *Microporous Mesoporous Mater.* **2008**, *115*, 123−136.
(26) Kirkpatrik, S.; Gelatt, C. D.; Vechhi, M. P. *Science* **1983**, *220* (4568), 671−680.
(27) Schwefel, H. P. *Numerical Optimization of Computer Models*; John Wiley & Sons: New York, 1981.
(28) Goldberg, D. E. *Genetic Algorithms in Search, Optimization, and Machine Learning*; Addison-Wesley: Reading, MA, 1989.
(29) Price, K.; Storn, R. *Dr. Dobb's J.* **1997**, *22*, 18−24.
(30) Babu, B. V.; Gaurav, C. In *Proceedings of International Symposium and 53rd Annual Session of IIChE (CHEMCON-2000)*, Science City, Calcutta, Dec. 18−21, 2000.
(31) Babu, B. V.; Angira, R. *Comput. Chem. Eng.* **2006**, *30*, 989−1002.
(32) Babu, B. V.; Munawar, S. A. *Chem. Eng. Sci.* **2007**, *62*, 3720−3739.
(33) Babu, B. V.; Sastry, K. K. N. *Comput. Chem. Eng.* **1999**, *23*, 327−339.
(34) Rahimpour, M. R.; Vakili, R.; Pourazadi, E.; Bahmanpour, A. M.; Iranshahi, D. *Int. J. Hydrogen Energy* **2011**, *36*, 3371−3383.
(35) Graaf, G. H.; Scholtens, H.; Stamhuis, E. J.; Beenackers, A. A. C. M. *Chem. Eng. Sci.* **1990**, *45*, 773−783.
(36) Graaf, G. H .; Sijtsema, P. J. J. M.; Stamhuis, E. J.; Joosten, G. E. H. *Chem. Eng. Sci.* **1986**, *41*, 2883−2890.
(37) Gallucci, F.; Paturzo, L.; Basile, A. *Ind. Eng. Chem. Res.* **2004**, *43*, 2420−2432.
(38) Price, K.; Storn, R. *J Global Optim.* **1997**, *11*, 341−359.
(39) Babu, B. V.; Angira, R. *Comput. Chem. Eng.* **2005**, *29* (5), 1041−1045.
(40) Lindsay, A. L.; Bromley, L. A. *Ind. Eng. Chem.* **1950**, *42*, 1508−1510.

(41) Cussler, E. L. *Diffusion, Mass Transfer in Fluid Systems*; Cambridge University Press: Cambridge, U.K., 1984.
(42) Wilke, C. R. *Chem. Eng. Progress* **1949**, *45*, 218−24.
(43) Reid, R. C.; Sherwood, T. K.; Prausnitz, J. *The Properties of Gases and Liquids*; McGraw-Hill: New York, 1977.
(44) Smith, J. M. *Chemical Engineering Kinetics*; McGraw-Hill: New York, 1980.
(45) Rahimpour, M. R.; Ghader, S. *Chem. Eng. Technol.* **2003**, *26* (8), 902−907.